Crimson Publishers
Wings to the Research

Research Article

Synthesis and Magneto-optical Properties of Co doped TiO_2 Nanotubes from Electro-spun Fiber Templates

Dickson M Andala[1]*, Samuel Chigome[2], Jermaine Omulami[3] and George O Achieng[4]

[1]Department of Chemistry, Multimedia University of Kenya, Kenya

[2]Botswana Institute for Technology Research and Innovation, Maranyane House, Plot 50654, Machel Drive, Private Bag 0082, Gaborone, Botswana

[3]Department of Chemistry, University of Nairobi, Kenya

[4]Department of Chemistry, Maseno University, Kenya

ISSN : 2688-8394

***Corresponding author:** Dickson M Andala, Department of Chemistry, Multimedia University of Kenya, P. O. Box 15653-00503, Nairobi, Kenya

Submission: September 12, 2023
Published: November 27, 2023

Volume 4 - Issue 3

How to cite this article: Dickson M Andala*, Samuel Chigome, Jermaine Omulami and George O Achieng. Synthesis and Magneto-optical Properties of Co doped TiO_2 Nanotubes from Electro-spun Fiber Templates. Ann Chem Sci Res. 4(3). ACSR. 000589. 2023. DOI: 10.31031/ACSR.2023.04.000589

Abstract

Submicron Co doped TiO_2 nanotubes were synthesized by the tubes by fiber template approach. Polymer fiber templates were fabricated by electrospinning while the tubes were synthesized by sol-gel deposition followed by thermal degradation of the polymer core. The diameters of the tubes ranged between ~350 ± 100nm with an average wall thickness of ~100 ± 50nm from SEM and TEM analysis. PXRD analysis indicated Co was homogenously distributed within substitutional sites of the polycrystalline anatase phase of the TiO_2. Photoluminescence studies confirmed n-type doping as indicated by reduction in intensity of highest energy direct photoemission (~420nm) due to charge transfer as well as presence of photoemission at (~470nm) associated with the presence of oxygen vacancies. Magnetic studies results indicated that the Co doped TiO_2 tubes were paramagnetic at room temperature.

Introduction

Titanium dioxide, a wide band gap semiconductor, has stimulated intense research interest due to its excellent optical transmission in the visible and near infrared region, high refractive index, high dielectric constant and useful photo catalytic properties [1]. As a result, it has found many interesting device applications such as photovoltaics, optics, magnetic storage, catalysis, sensors and battery electrodes [2-4]. More recently, Co doped titanium oxide has stimulated intense and broad studies both in theory and experimental as a dilute magnetic semiconductor following discovery of robust, room temperature ferromagnetism important in spintronics [5,6].

The fabrication of dilute magnetic semiconductors has been achieved using several deposition techniques including oxygen assisted molecular beam epitaxy, pulsed laser deposition, solid vapor deposition/co-sputtering, ion implantation and cathodic electrolytic deposition [5,7-9]. However, these methods are not only expensive but less straightforward hence have limitations in terms of throughput. Similarly, the origin of room temperature ferromagnetism still remains controversial in dilute magnetic semiconductors prepared by these techniques in reducing environments or ultra-high vacuum because of the possibility of segregation of transition metal particles resulting in phase separation [10].

Currently, endeavour's particularly focused on wet chemical synthesis under suitable conditions have proved quintessential in addressing these limitations while aiding in understanding the origin of ferromagnetism. Consequently, not only a single phase of Co doped TiO_2 polycrystalline are produced but also allows for integration with Si technology that is important in spintronics [10,11]. In this work Co doped TiO_2 nanotubes were prepared by the

tubes by fiber templating technique via a Sol-gel process. Electro-spun fibers served as templates which on thermal degradation yielded hollow Co-TiO_2 nanotubes [12,13]. Electrospinning is a technique that relies on repulsive electrostatic forces to produces solid fibers in the nanometre to micro-meter range from polymer solutions or melts [14]. The forces to offers unique advantages for preparing homogenous multicomponent oxides compared to gas phase techniques [15].

The Co doped TiO_2 were characterized for magnetic and optical properties relative to thin films obtained by molecular beam epitaxy and co-sputtering techniques. Similarly, magneto-optical properties of Co doped TiO_2 nanotubes were of importance since most studies reported have focused on 2 dimensional materials, thin films. The tubular structure of these Co doped TiO_2 nanotubes becomes particularly important due to its high aspect ratio, high porosity and the quantum confinement effects as a result of reduction in dimensions.

Experimental Section

Materials

Polylactide (PLA) pellets (Mwt. 180,000), Polycarbonate pellets (Mwt. 64,000) methylene chloride, N, N-dimethylformamide (DMF), Tin Chloride Palladium Chloride, Cobalt (II) nitrate hexahydrate, Titanium isopropoxide (TiP), 2-propanol and Hydrochloric acid all from Sigma-Aldrich were used as received.

Electrospinning and Sol-gel deposition

The template fibers were prepared by electrospinning polylactide or polycarbonate polymer solution. The polymer solutions were prepared by dissolving 180mg/mL in dichloromethane/dimethylformamide (0.65/ 0.35) solvent mixture. Electrospinning was done at 20kV (applied voltage) with a working distance of 20cm between the collector screen and the spinneret [14]. The electro-spun fibers were peeled off from the aluminium foil collector screen after soaking in 1M HCl solution and then rinsed in deionized water prior to use.

Titanium oxide polylactide coaxial fibers were fabricated via wet chemical synthesis through the hydrolysis of titanium isopropoxide, TiO_2 precursor, followed by condensation in the sol-gel deposition process. The template was first sensitized and then activated by immersion in 3.0mM $PdCl_2$ aqueous solution containing 0.01M HCl. The colloidal suspension for Co doped TiO_2 nanotubes was prepared using Titanium isopropoxide (TiP) as TiO_2 precursor and Cobalt (II) Nitrate hexahydrate as the dopant source. Under constant stirring, 1.0mL of TiP was added drop wise to a 20mL solution of 0.01M (0.055g) Cobalt (II) Nitrate hexahydrate in 2-propanol. The resulting mixture was stirred for 2h over an ice bath to form a homogenous and stable colloidal solution. The percent dopant loading was varied by varying the concentration of $Co(NO_3)_2.6H_2O$ used.

Activated and sensitized template fibers were immersed into the colloidal suspension and the reaction proceeded with constant stirring for 2h over an ice bath resulting in a coating of Co-TiO_2. After coating, the fibers were removed from the colloidal suspension and allowed to hydrolyze in air of 24h at room temperature. This resulted in gelation and formation of PLA-Co-TiO_2 coaxial fibers. The coaxial fibers were then calcined in air at 500 °C at a ramp rate 10 °C/min and annealed at that temperature for 3h.

Instrumentation

The morphology, dimensions and elemental composition of the synthesized materials were characterized by electron microscopy. Scanning Electron Microscope (SEM) model Hitachi S-570LB equipped with an Energy Dispersive Spectroscopy (EDS) was used. For morphological studies lower acceleration voltage of 5kV was applied while for EDS 15-20kV was used. For non-conducting samples a thin film of Au/Pd was coated on the surface prior to taking image. Transmission electron microscopy (TEM) was performed on Hitachi 2000 TEM instrument. Thermogravimetric Analysis (TGA) was performed on TA 2950 Analyzer.

The electronic and crystal structure was analyzed using spectroscopic techniques. Electronic absorption spectra were recorded on a Hewlett Packard 8452A UV-visible spectrophotometer. Infra-red spectra were recorded on a digilab FTS-40 PRO as a KBr pellet or fiber mat. The X-ray diffraction spectra were measured on finely ground tubes using Scintag X-ray diffractometer with X-ray wavelength f 1.5418 Å (Cu Kα) radiation source. The samples for PXRD were smoothly ground and compacted to at least 1mm in thickness to prevent penetration of the X-ray beam. The crystalline size was estimated by applying the Scherrer equation to the FWHM of the (101) peak of anatase.

Magnetic properties were determined on a Superconducting Quantum Interference Device (SQUID) magnetometer, Quantum Design MPMS XL-5. The magnetic susceptibility (χ=M/H, M is magnetization, H is applied magnetic field) of the samples was measured from 2 to 400 K in a magnetic field of 1000 Oe. Magnetization curves were measured at 298K in magnetic fields up to 5T. The samples were zero-field-cooled to 5K before the magnetization measurements.

Results and Discussion

Tubes by fiber templating and material characterization

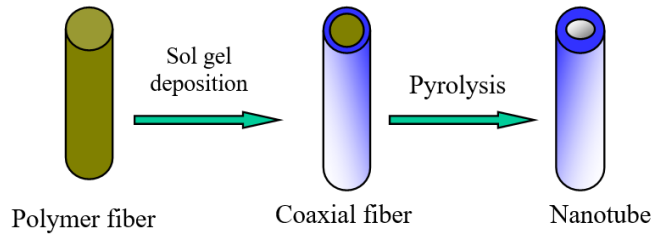

Scheme 1: Schematic diagram of tubes by fiber template process

Templating remains one of the most rapidly growing areas of research in materials synthesis. It entails fabrication of structured materials over a scaffold material, template, such as electro-spun fibers. The removal of the template by thermal treatment generates the desired structure in this case submicron tubes as shown in scheme 1 [12,16,17]. The template-based approach provides

a versatile and a low-cost method of preparing nanometer to submicron materials in high volume and with better control of dimension and surface morphology from nanometer to submicron length scale templates.

Sol-gel technology is an attractive methodology for the design and synthesis of advanced ceramic material with anisotropic properties through the control of both the structure and chemistry of the materials. In particular, doping metal oxides with transition metal ions modifies crystalline structure which determines the physical and chemical properties of these materials [10,11]. Sol-gel technology offers the advantage of low cost, low processing temperatures, and potential for highly homogenous and quality deposits [17].

The electrospun PLA or PC nanofibers were preferred as templates materials with CH_2Cl_2 and DMF as solvents since they both have a good solubility in methylene dichloride (CH_2Cl_2). DMF was used as a co-solvent to increase jet stability against decomposition under a high electric field since it has a high dielectric constant. The morphology of PLA fibers was examined using Scanning Electron Microscopy (SEM), revealed that the surfaces were smooth and uniform without beads with an average diameter around 250±100nm, Figure 1.

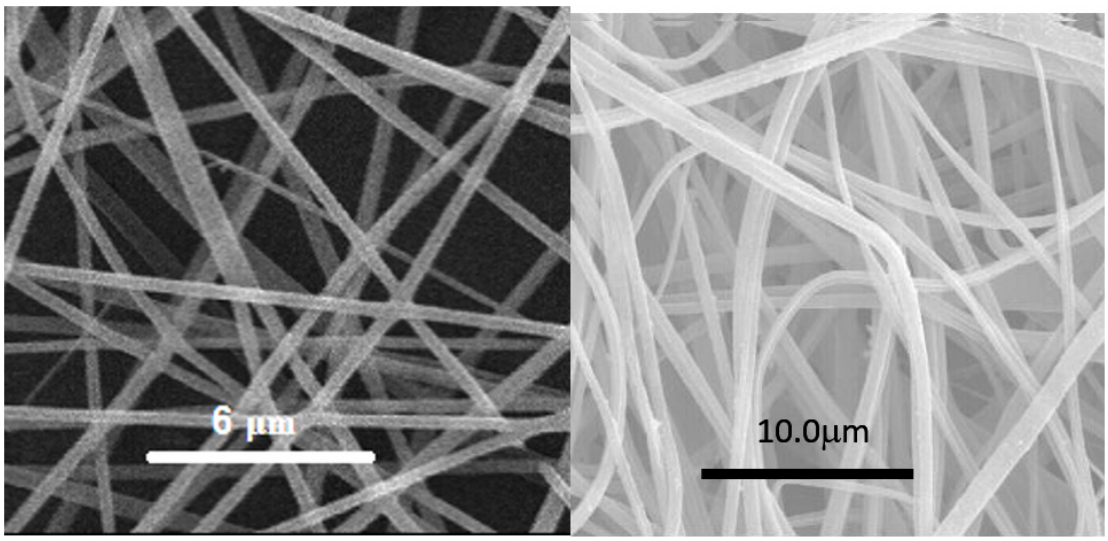

Figure 1: SEM image of electrospun PLA template fibers (a) Polycarbonate fibers (b).

PLA was selected as template material based on its favorable stability and relatively low decomposition temperature 235-255 °C as confirmed by Thermogravimetric Analysis [18] Figure(2a,2b). Low decomposition temperature was important in reducing cross linking of titanium oxide tubes during thermal treatment. From the TGA curve of PLA/TiO_2 coaxial fibers, the initial weight loss around 100 °C to 260 °C was attributed to loss of solvent, decomposition of titanium isopropoxide and decomposition of polylactide. There was no further weight loss after 300 °C indicating the formation of TiO_2 tubes.

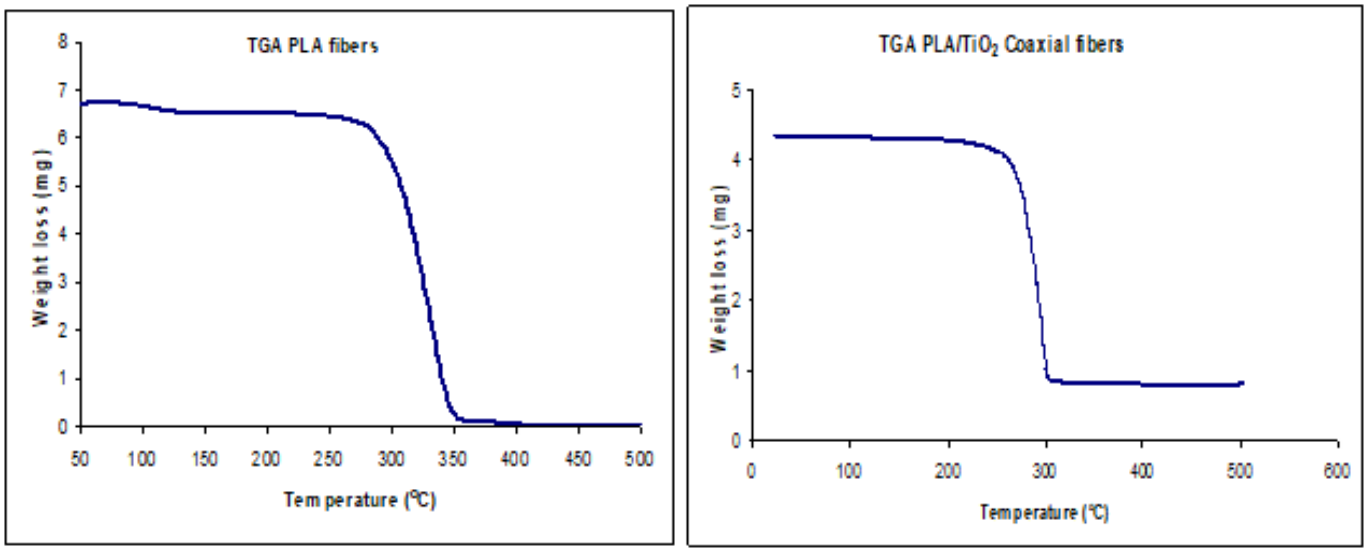

Figure 2: Thermogravimetric Analysis of PLA fibers (a) PLA/TiO_2 coaxial fibers (b).

The sol-gel deposition procedure employed was simpler than established gas phase methods, since the sols consisted of only three components: titanium isopropoxide precursor, Cobalt (II) nitrate hexahydrate as the dopant, and 2-propanol as solvent. Since titanium isopropoxide and $Co(NO_3)_2.6H_2O$ were highly soluble in 2-propanol hence no heating was necessary for the starting mixture. Heating the sol precursors increases the possibility of inadvertently altering the oxidation state of the dopants or forming dopant oxide secondary phases prior to TiO_2 deposition, as confirmed by PXRD. In addition, no additive was required to improve sol stability and homogeneity. This favored an even drying and uniaxial crystallization of TiO_2 from SEM characterization.

The resultant PLA-Co-TiO_2 coaxial fibers obtained were found to have a larger diameter compared to PLA template fibers from electron microscopy studies. Figure 3 shows the SEM of PLA-Co-TiO_2 coaxial fibers with diameters ranging between 450 ± 100nm. Thermal degradation of PLA template core yielded hollow Co-TiO_2 nanotubes with diameters ranging between 350 ± 100nm, Figure 4. The wall thickness of the tubes ranged between 100 ± 50nm. The decrease in tube diameter relative to coaxial fibers was attributed to crystallization of TiO_2. TEM images and electron diffraction pattern confirmed the tubes were hollow as opposed to solid nanowires and polycrystalline in structure respectively Figure 5. Figure 6 represents an EDS spectrum of Co doped TiO_2 nanotubes, Ti and O peaks are consistent with formation of TiO_2 after thermal treatment. The Co peak was attributed to the addition of cobalt nitrate during the sol-gel process as a dopant.

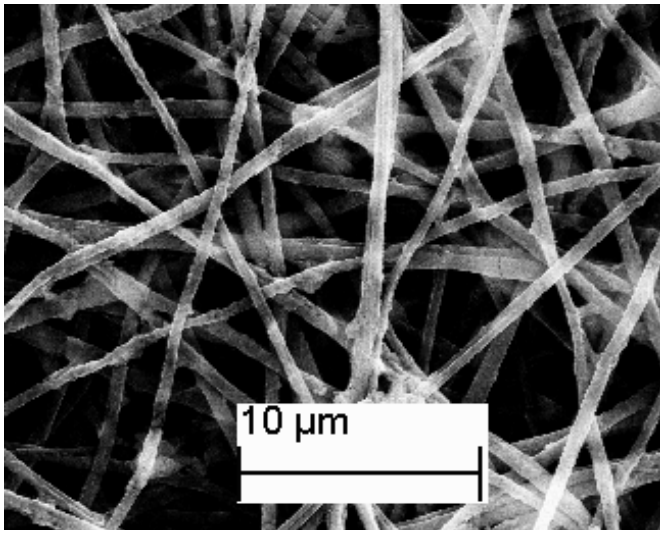

Figure 3: SEM image of electrospun Co-TiO_2/PLA coaxial fibers.

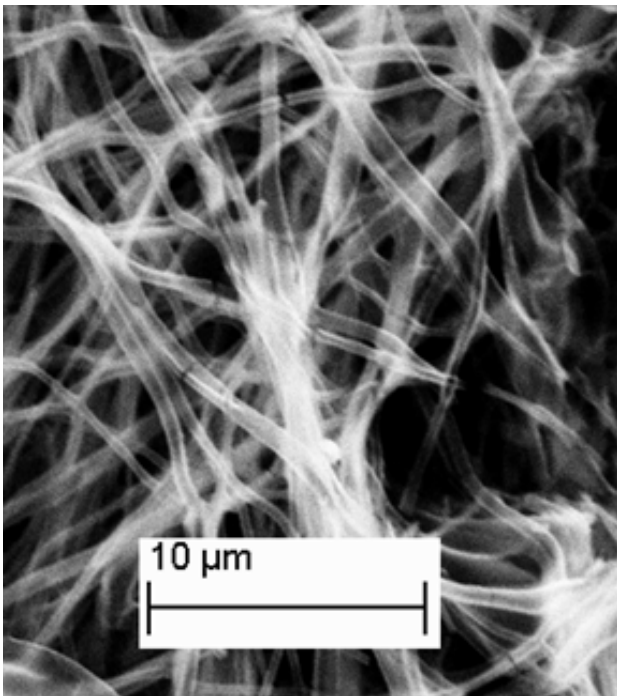

Figure 4: SEM image of electrospun Co doped TiO_2 nanotubes.

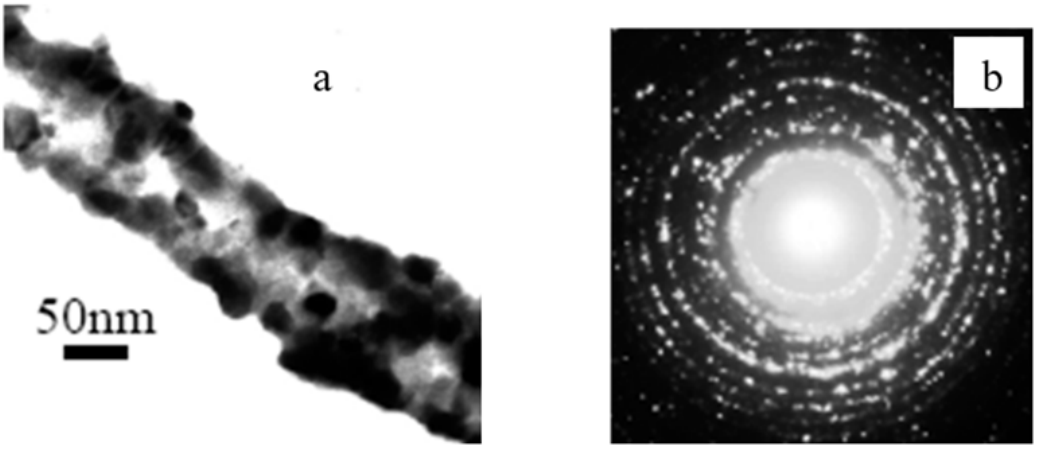

Figure 5: (a) TEM image of Co doped TiO_2 indicating it has a hollow interior (b) Electron diffraction pattern for Co doped TiO_2 indicating polycrystallinity.

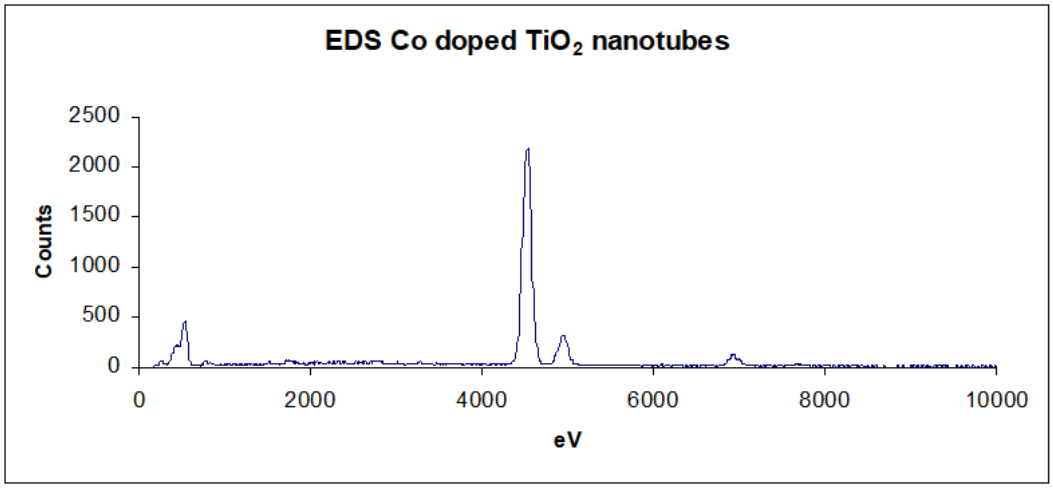

Figure 6: EDS spectrum for Co-TiO_2 nanotubes.

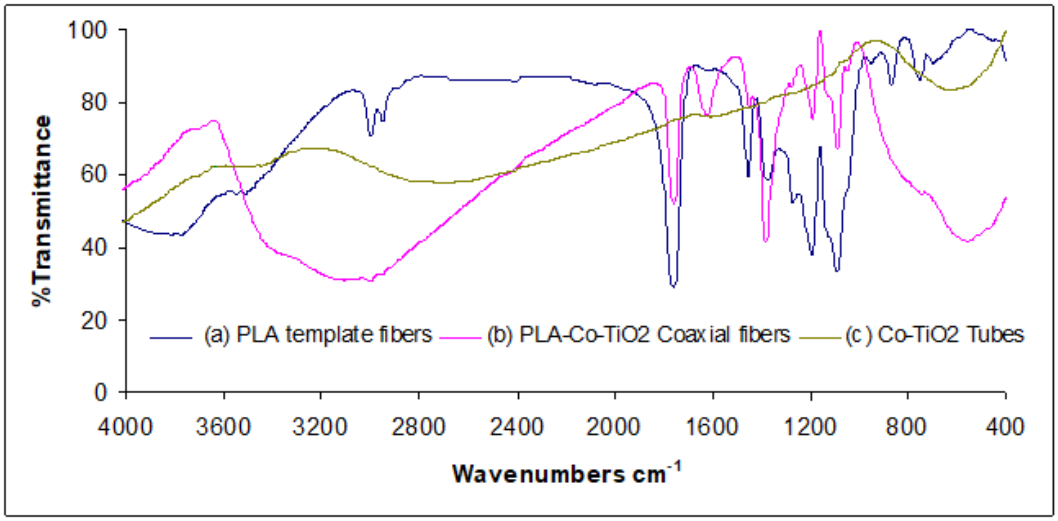

Figure 7: FTIR spectra of PLA template, PLA-Co-TiO_2 coaxial fibers and Co doped TiO_2 tubes after thermal treatment.

Infrared spectroscopy was similarly instrumental in determination of complete elimination of the template core following thermal degradation. Figure 7(a) shows the FTIR spectrum of neat polylactide template fibers prior to sol-gel deposition. The broad absorption bands at ~3800-3500cm^{-1} corresponded to stretching vibrations of OH groups. The sharp bands at ~3000-2950cm^{-1}

were assigned to the stretching vibration of aliphatic CH_3 groups. The strong vibrations at 1766cm^{-1} were due to ν(C=O) stretch while those at 1458cm^{-1} and in the range 1200–1000cm^{-1} were assigned to C-C and C-O stretching vibrations respectively [18,19]. PLA-Co-TiO_2 coaxial fibers FTIR spectrum, Figure 7b, exhibited similar characteristic features of the template except for the new bands at ~1624cm^{-1} corresponding to isopropoxide groups bonded to titanium, indicating the isopropoxide groups remain bonded during the sol-gel process. The broadened band ~500-700cm^{-1} was assigned to ν(Ti-O) lattice vibrations. On thermal treatment, these vibrations disappeared indicating decomposition of the polymer template material, with no sign of polylactide nor isopropoxide organic residues. The resultant broad absorption band between 500-700cm^{-1} was assigned to ν(Ti-O) lattice vibrations, Figure 7(c) [20].

Structural properties and crystallite size of synthesized material was obtained by X-ray diffraction experiments. The as prepared Co-doped coaxial fibers were amorphous and on thermal treatment at 500 °C diffraction peaks attributed to anatase crystalline phase of TiO_2 were obtained [21]. The observed diffraction planes were 2θ=25.04°(101), 37.96°(103,004,112), 47.88°(200), 54.64°(211), 62.94°(204), 69.48°(116,220), 75.66°(215) corresponding to the miller indices in parenthesis. A comparison with standard diffraction spectrum, JCPDS card 21-1272 resulted in a good match with the experimental diffraction pattern. Moreover, no evidence of cobalt [22], cobalt oxide [23] or Co-Ti oxide phases, which are known to exist in bulk Co-Ti-O phase diagram were obtained [24]. This result seems to support the hypothesis that Co was distributed homogeneously in substitutional sites of anatase TiO_2 matrix. The average crystallite size was 16.28nm as estimated using the Scherrer's equation.

Doping of TiO_2 with transition metal ions has been shown to influence TiO_2 structure depending on the concentration of the dopant. In this case, a low concentration of Co prevented it from segregating (surface nucleation) on the surface of TiO_2, which inhibits sintering of amorphous TiO_2 particles. The absence of a mixed phase, due to effective segregation, indicates Co was homogenously distributed within substitutional sites of the anatase matrix [15]. The influence of the dopant on the structural and textural properties of the samples can be explained based on the changes caused by the dopant on the defect structure of TiO_2 lattice; these changes are strongly dependent on the charge and size of the dopant ion [25,26]. Since, PXRD gives only the average crystal structure, the presence of crystal defects or impurities were determined from photoluminescence and magnetic studies (Figure 8).

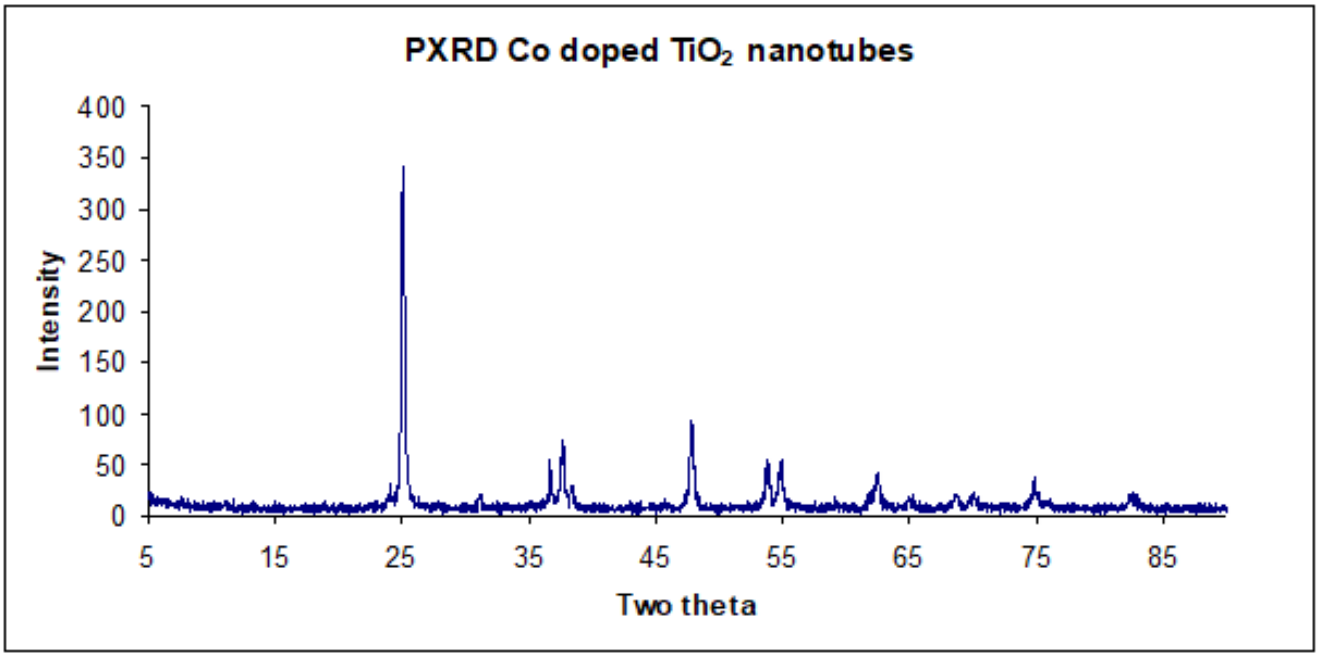

Figure 8: PXRD pattern of TiO_2 nanotubes doped with Co calcined at 500 °C.

Optical and Magnetic properties

The changes in TiO_2 band structure were investigated using UV-visible spectroscopy. The absorption maximum for Co doped TiO_2 nanotubes occurred around 325nm, Figure 9. This compared well with the absorption spectrum of neat TiO_2, however there was no abrupt absorption edge similar to TiO_2 nanotubes. The smearing of the band edge may be attributed to the presence of Co impurities within TiO_2 matrix [17]. Broadening results due to vibronic coupling between the valence electrons of dopant (Co) and TiO_2 phonons (lattice vibrations).

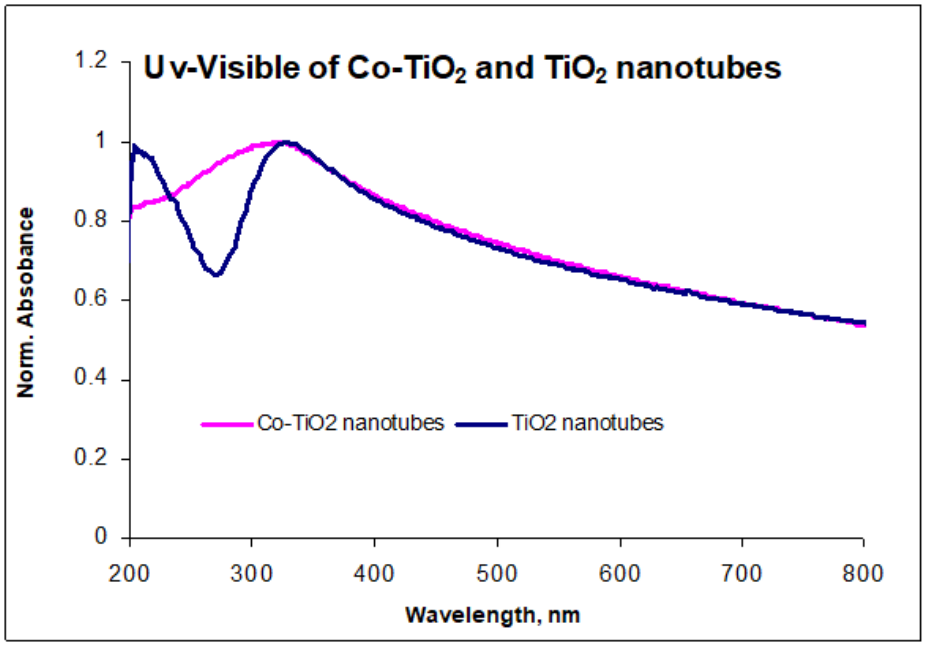

Figure 9: UV-visible spectrum of Co doped TiO_2 nanotubes.

The maximum absorption for TiO_2 nanotubes was similarly blue shifted relative to macro-crystalline TiO_2 which normally occurs around 380nm. The band gap widening was due to quantum confinement effects as a result of downsizing which is in agreement with literature studies on TiO_2 nanostructures [27,28]. Co doping was expected to shift the absorption edge of TiO_2 nanotubes to longer wavelength consistent with charge-transfer transition between the d-electrons of the dopant and the TiO_2 conduction band, n-type doping. The fact that the band gap did not decrease relative to TiO_2 nanotubes was likely due to strong band broadening, rendering precise determination of the band gap difficult, as indicated in literature for doped semiconductors [29,30]. Absorption band edge becomes more diffuse due to increasing disorder and change in lattice constant due to doping. The absence of red shift in band edge was not unique since theoretical band gap calculations for doped anatase predict the energy gap between conducting band (O 2p) and valence band (Ti 3d states) to remain unchanged on doping [31].

Photoluminescence studies provided fundamental information on energy levels lying within the band gap relative to the UV-visible absorption spectrum. The emission spectrum of Co-TiO_2 nanotubes was obtained by using excitation wavelength of 325nm in the range of 350-600nm at room temperature. This spectrum exhibited three emission peaks located at 374nm, 420nm and 470nm, Figure 10. The emission transition at 374nm and 420nm were attributed to highest energy direct photoemission band gap and the lowest energy indirect transition respectively [27,32]. The reduction in intensity observed in Co-TiO_2 nanotubes direct transition with Co doping is ascribed to the introduction of Co^{2+} 3d states in the conduction band. This is consistent with charge-transfer transition between the d-electrons of the dopant and the TiO_2 conduction band, n-type doping [33].

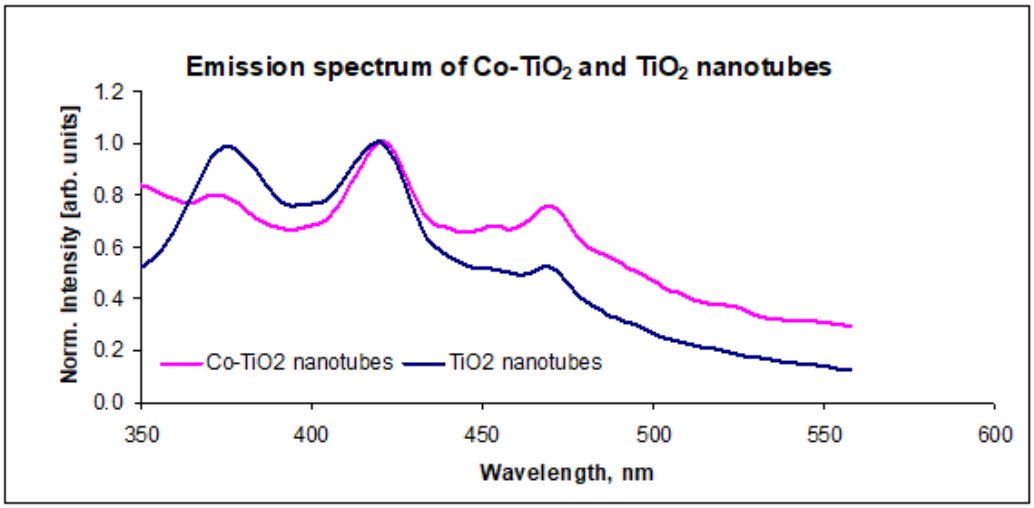

Figure 10: Emission spectrum of Co doped TiO_2 nanotubes.

The emission band at 470nm could be attributed to physical origins within the band gap: self-trapped excitons and oxygen vacancies [32,34]. For pure TiO_2 nanotubes, this transition was assigned to the recombination of self-trapped excitons localized within TiO_2 octahedra. The self- trapped excitons originate from band-to-band excitation where the excited electron and the remaining hole create a local deformation of TiO_2 octahedra and thus localize themselves into a state in the energy gap of TiO_2. In the case of Co doped TiO_2 nanotubes a combination of both factors for this emission peak (470nm), consistent with increase in peak intensity. This transition is assigned to self-trapped excitons similar to that of TiO_2 nanotubes and photoluminescence due to oxygen vacancies. The oxygen vacancies are created following substitution of Ti^{4+} by Co^{2+} in the lattice in order to maintain neutrality [32,34]. Cation dopants with a charge of +4 or lower have been reported to reduce or increase the oxygen vacancy concentration in TiO_2 depending on their position in the lattice. If the dopant ions (Co^{2+}) substitute Ti^{4+} ions, oxygen vacancies tend to increase, but if they are put in interstitial positions, the oxygen vacancy concentration decreases, lowering on crystal defects and phase transformation [15,17]. The broadening of the emission band with tailing to lower energy was attributed to broad polycrystalline size distribution and Co impurity [35].

Magnetic characterization was performed on Co-TiO_2 nanotubes at room temperature. The dopant concentration was similarly varied to determine the dependence of magnetization on Co content. Figure 11 shows the results of magnetic susceptibility as a function of temperature for Co doped TiO_2 nanotubes. Low concentrations of Co below 4% resulted in uniform solid solution curve A, as the concentration of Co dopant increased a magnetic phase transition was observed at 38K (curve B). This was attributed to formation of $CoTiO_3$ impurity with a Néel temperature of 38K, corresponding to antiferromagnetic-paramagnetic transition [36]. The observed transition temperature was independent of Co content and magnetic field applied consistent with formation of magnetically ordered $CoTiO_3$ phase.

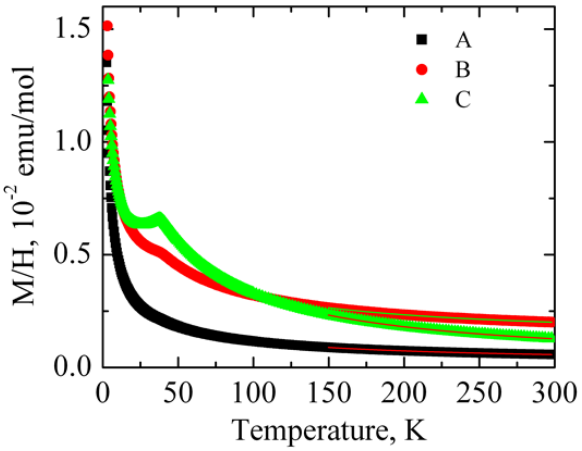

Figure 11: Magnetic susceptibility curve for Co-TiO_2 nanotubes.

The inverse plot ($1/\chi$ vs T) follows Curie-Weiss behavior above 150K with C= 0.13 (1) emuK/mol, Curie-Weiss temperature of Q = -38 (2) K, for sample A with lowest Co content. This corresponded to 3.5 to 4.3% Co^{2+} ions with moderate antiferromagnetic exchange, Figure 12. This compared well with the EDS estimate of Co^{2+} concentration of about 5.2-6.3% from elemental mapping of Co doped TiO_2 nanotubes. For a detailed description of each sample see Table 1.

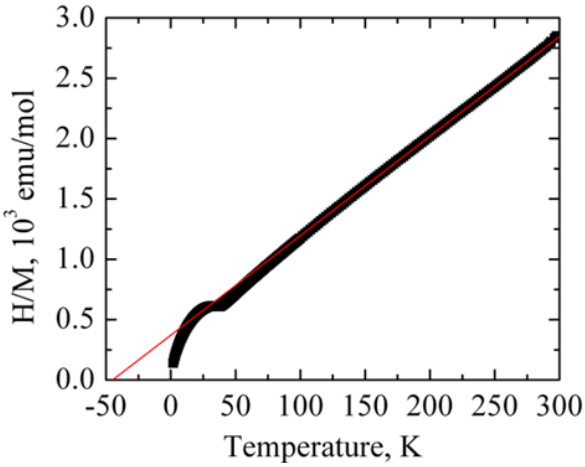

Figure 12: Curie-Weiss plot, indicating Curie-weiss temperature (sample A).

Table 1: Magnetic properties of Co-TiO_2 tubes.

Sample	38 K transition	χ0, 10-4 emu/mol	C, emu K/mol	Θ, K	Co^{2+}, mol.% μ eff = 3.87 μ B	Co^{2+}, mol.% μ eff = 4.7 μ B	Co^{2+}, mol.% μ eff = 5.2 μ B
A	No	1.8	0.13(1)	-38	6.9	4.7	3.8
B	Yes	12.6	0.24(1)	-24	12.8	8.7	7.1
C	Yes	1.2	0.36(1)	-15	19.2	13	10.7

Figure 12 shows 298K hysteresis loop measured for Co-TiO_2 (A), without magnetic phase transition. The linear dependence of magnetization on magnetic field and the absence of a magnetic hysteresis loop indicates Co doped TiO_2 nanotubes prepared were paramagnetic at lower percent loadings. The absence of room temperature ferromagnetism in Co doped TiO_2 nanotubes may be attributed to calcination in air which may have favoured formation of larger fraction of antiferromagnetically coupled Co^{2+} ions resulting in negligible contribution to overall magnetization [36,37] Figure 13.

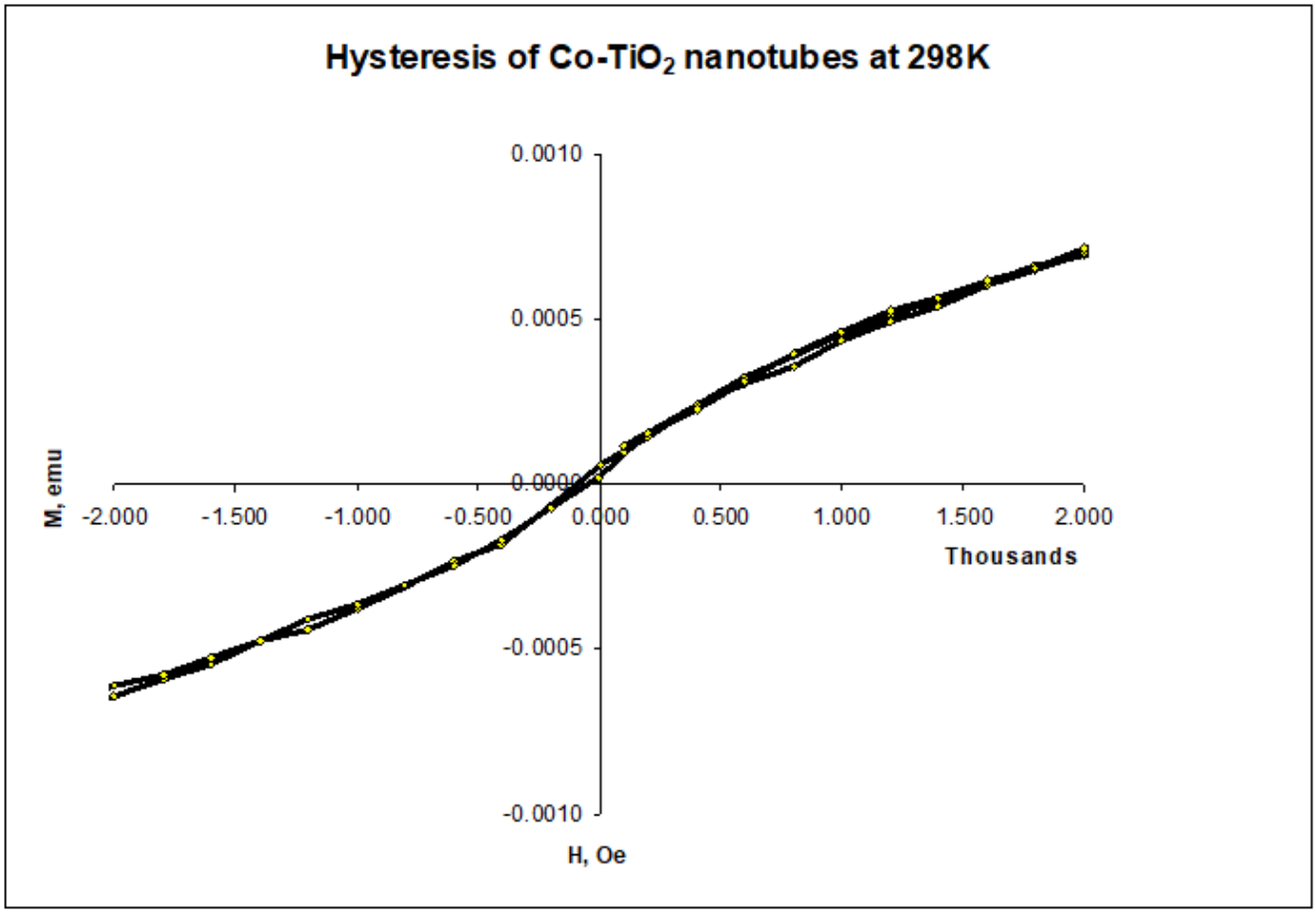

Figure 13: Hysteresis loop for Co-TiO_2 nanotubes, sample A.

Conclusion

Co doped TiO_2 submicron tubes were fabricated using electro-spun polymer fibers as templates via Sol-gel deposition. Thermal degradation of the template core at 500 °C resulted in polycrystalline anatase TiO_2 tubes with Co distributed within substitutional sites. UV-visible measurements indicated band gap widening due to quantum confinement effects, while photoluminescence experiments confirmed presence of point defects due to oxygen vacancies. Magnetization measurements indicated Co doped TiO_2 nanotubes were paramagnetic with a magnetic phase transition occurring reported in samples with higher than 4% Co loading. Future studies will focus on improving magnetic ordering and application these structures in spintronics.

References

1. Diebold U (2003) The surface science of titanium dioxide. Surface Science Reports 48(5-8): 53-229.
2. Hayakawa I, Iwamoto Y, Kikuta K, Hirano S (2000) Gas sensing properties of platinum dispersed-TiO_2 thin film derived from precursor. Sensors and Actuators B: Chemical 62(1): 55-60.
3. Dai XC, Zhang X, Ding X, Wang X, Liu, P, et al. (2009) ChemPhysChem 10(8).
4. Zhu YSJ, Zhang Z, Zhang C, Zhang X (2002) Analytical Chemistry 74(4).

5. Matsumoto Y, Takahashi R, Murakami M, Koida T, Fan XJ, et al. (2001) Ferromagnetism in Co-Doped TiO_2 rutile thin films grown by laser molecular beam epitaxy. Japanese Journal of Applied Physics 40(11B): L1204-L1206.
6. Matsumoto Y, Murakami M, Shono T, Hasegawa T, Fukumura T, et al. (2001) Room-temperature ferromagnetism in transparent transition metal-doped titanium dioxide. Science 291(5505): 854-856.
7. Ueda K, Tabata H, Kawai T (2001) Room-temperature ferromagnetism in transparent transition metal-doped titanium dioxide. Applied Physics Letters 79: 988-990.
8. Kim YJ, Thevuthasan S, Droubay T, Lea AS, Wang CM, et al. (2004) Growth and properties of molecular beam epitaxially grown ferromagnetic Fe-doped TiO_2 rutile films on TiO_2. Applied Physics Letters 84(18): 3531-3533.
9. Stampe PA, Kennedy RJ, Xin Y, Parker JS (2003) Investigation of the cobalt distribution in the room temperature ferromagnet TiO_2 : Co. Journal of Applied Physics 93(10): 7864-7866.
10. Punnoose A, Hays J, Gopal V, Shutthanandan V (2004) Room-temperature ferromagnetism in chemically synthesized $Sn_{1-x}Co_xO_2$ powders. Applied Physics Letters 85(9): 1559-1561.
11. Nunes RMMCO, Castro LA, Vasconcelos AD, Silvestre JA (2008) European Journal of Inorganic Chemistry 2008(4).
12. Ochanda F, Jones WE (2005) Sub-Micrometer-Sized metal tubes from electrospun fiber templates. Langmuir 21(23): 10791-10796.
13. Yarin AL, Koombhongse S, Reneker DH (2001) Bending instability in electrospinning of nanofibers. Journal of Applied Physics 89(5): 3018-3026.
14. Dong H, Nyame V, Macdiarmid AG, Jones WE (2004) Polyaniline/poly(methyl methacrylate) coaxial fibers: The fabrication and effects of the solution properties on the morphology of electrospun core fibers. Journal of Polymer Science Part B-Polymer Physics 42(21): 3934-3942.
15. Arroyo R, Cordoba G, Padilla J, Lara VH (2002) Influence of manganese ions on the anatase–rutile phase transition of TiO_2 prepared by the sol–gel process. Materials Letters 54(5-6): 397-402.
16. Martin CR (1996) Membrane-Based synthesis of nanomaterials. Chemistry of Materials 8(8): 1739-1746.
17. Ochanda F, Cho K, Andala D, Keane TC, Atkinson A, et al. (2009) Synthesis and optical properties of Co-Doped ZnO submicrometer tubes from electrospun fiber templates. Langmuir 25(13): 7547-7552.
18. Engelberg I, Kohn J (1991) Physico-mechanical properties of degradable polymers used in medical applications: a comparative study. Biomaterials 12(3): 292-304.
19. Zhang J, Luo SC, Gui LL (1997) Poly(methyl methacrylate)–titania hybrid materials by sol–gel processing. Journal of Materials Science 32: 1469-1472.
20. Skotak M, Larsen G (2006) Solution chemistry control to make well defined submicron continuous fibres by electrospinning: the $(CH_3CH_2CH_2O)_4$Ti/AcOH/poly(*N*-vinylpyrrolidone) system. Journal of Materials Chemistry 16: 3031-3039.
21. Watthanaarun J, Pavarajarn V, Supaphol P (2005) Titanium (IV) oxide nanofibers by combined sol–gel and electrospinning techniques: preliminary report on effects of preparation conditions and secondary metal dopant. Science and Technology of Advanced Materials 6(3-4): 240-245.
22. Crowley TA, Ziegler KJ, Lyons DM, Erts D, Olin H, et al. (2003) Synthesis of metal and metal oxide nanowire and nanotube arrays within a mesoporous silica template. Chemistry of Materials 15(18): 3518-3522.
23. Feifei Tao CG, Zhenhai Wen, Quiang Wang, Jinhong Li, Zheng Xu (2009) Cobalt oxide hollow microspheres with micro- and nano-scale composite structure: Fabrication and electrochemical performance. Journal of Solid State Chemistry 182(5): 1055-1060.
24. Yankin A, Vikhreva O, Balakirev V (1999) *P*–*T*–*x* diagram of the Co–Ti–O system. Journal of Physics and Chemistry of Solids 60(1): 139-143.
25. Al-Salim NI, Bagshaw SA, Bittar A, Kemmitt T, McQuillan AJ, et al. (2000) Characterisation and activity of sol-gel prepared TiO_2 photocatalysts modified with Ca, Sr or Ba ion additives. Journal of Materials Chemistry 10(10): 2358-2363.
26. Vargas S, Arroyo R, Haro E, Rodriguez R (1999) Effects of cationic dopants on the phase transition temperature of titania prepared by the sol-gel method. Journal of Materials Research 14: 3932-3937.
27. Bavykin DV, Gordeev SN, Moskalenko AV, Lapkin AA, Walsh FC (2005) Apparent two-dimensional behavior of TiO_2 nanotubes revealed by light absorption and luminescence. Journal of Physical Chemistry B 109(18): 8565-8569.
28. Li Y, White TJ, Lim SH (2004) Low-temperature synthesis and microstructural control of titania nano-particles. Journal of Solid State Chemistry 177(4-5): 1372-1381.
29. Salvador P (1980) The influence of niobium doping on the efficiency of n-TiO_2 electrode in water photoelectrolysis. Solar Energy Materials 2(4): 413-421.
30. Mark F (2001) Optical Properties of Solids. Oxford University Press, London.
31. Park MS, Kwon SK, Min BI (2002) Electronic structures of doped anataseTiO_2:$Ti_{1-x}M_xO_2$(M=Co, Mn, Fe, Ni). Physical Review B 65(16): 161201.
32. Lai YK, Sun L, Chen C, Nie CG, Zuo J, et al. (2005) Optical and electrical characterization of TiO_2 nanotube arrays on titanium substrate. Applied Surface Science 252(4): 1101-1106.
33. Wang XH, Li JG, Kamiyama H, Katada M, Ohashi N, et al. (2005) Pyrogenic Iron(III)-Doped TiO_2 nanopowders synthesized in rf thermal plasma: Phase formation, defect structure, band gap, and magnetic properties. Journal of the American Chemical Society 127(31): 10982-10990.
34. Jia CW, Xie EQ, Zhao JG, Duan HG, Zhang YZ (2007) Annealing temperature dependence of ferromagnetism in Co-doped TiO_2 nanofibres. Materials Science and Engineering B 140(1-2): 10-14.
35. Schwartz DA, Norberg NS, Nguyen QP, Parker JM, Gamelin DR (2003) Magnetic quantum dots: Synthesis, spectroscopy, and magnetism of Co^{2+}- and Ni^{2+}-Doped ZnO nanocrystals. Journal of the American Chemical Society 125(43): 13205-13218.
36. Fleischhammer M, Panthofer M, Trernel W (2009) The solubility of Co in TiO_2 anatase and rutile and its effect on the magnetic properties. Journal of Solid-State Chemistry 182(4): 942-947.
37. Bryan JD, Heald SM, Chambers SA, Gamelin DR (2004) Strong room-temperature ferromagnetism in Co^{2+}-Doped TiO_2 made from colloidal nanocrystals. Journal of the American Chemical Society 126(37): 11640-11647.